
A COMPACT FOURTH-ORDER IMPLICIT-EXPLICIT RUNGE-KUTTA TYPE SCHEME FOR NUMERICAL SOLUTION OF THE KURAMOTO-SIVASHINSKY EQUATION

A PREPRINT

Harish Bhatt
Center for Student Success and Retention
Savannah State University
Savannah, GA 31404
bhatth@savannahstate.edu

Abhinandan Chowdhury
Department of Mathematics
Savannah State University
Savannah, GA 31404
chowdhury@savannahstate.edu

March 13, 2024

ABSTRACT

This manuscript introduces a fourth-order Runge-Kutta based implicit-explicit scheme in time along with compact fourth-order finite difference scheme in space for the solution of one-dimensional Kuramoto-Sivashinsky equation with periodic and Dirichlet boundary conditions, respectively. The proposed scheme takes full advantage of method of line (MOL) and partial fraction decomposition techniques, therefore it just need to solve two backward Euler-type linear systems at each time step to get the solution. Performance of the scheme is investigated by testing it on some test examples and by comparing numerical results with relevant known schemes. It is found that the proposed scheme is more accurate and reliable than existing schemes to solve Kuramoto-Sivashinsky equation.

Keywords Implicit-explicit scheme; Kuramoto-Sivashinsky equation; Partial fraction splitting technique; Compact finite difference; Exponential time differencing

1 Introduction

The present study is concerned with the development and the implementation of a numerical scheme to solve well-known Kuramoto-Sivashinsky equation (KSE - for brevity) 1 with appropriate initial and boundary conditions. The KSE is the equation governing in the frame of the weakly nonlinear approximation for the shape of the free surface of thin film of viscous liquid falling down a vertical plane when the capillary forces are substantial. Kapitza in his pioneering work [19] first investigated the role of viscosity on the capillary flow in thin layers. Benny [5] carried out the boundary-layer simplifications for the viscous case and Homsy [17] developed the long-wave weakly-nonlinear approximation whose consistent application allows one to derive the following dimensionless equation for evolution of the scaled film thickness u , after rescaling the variables

$$u_t + uu_x + \alpha u_{xx} + \beta u_{xxxx} = 0, \quad (1)$$

where α and β are nonzero constants. The Eq. 1 are usually referred as KSE which is of great fundamental interest just in the same way as its famous counterparts Korteweg-de Vries (KdV) and Burgers equations are. The alternative form of KSE was obtained in [24] while deriving it as a phase equation for the complex Ginzburg-Landau equation for the evolution of reaction fronts. The KSE also describes flame-front instabilities [35, 36, 12] as well as the dynamics of viscous-fluid films flowing along walls [37, 34]. For more details associated with the rich phenomenology of this flow, we refer the reader to [4] and [33] for comprehensive reviews of the experimental and theoretical approaches, respectively.

The KSE is a nonlinear evolution equation which is capable of demonstrating chaotic behavior in both time and space. It contains nonlinearity, fourth-order dissipative term u_{xxxx} and second-order source term u_{xx} (anti-dissipation). In

fact, the KSE represents the extreme case when the dispersion is negligible in comparison with dissipation while the KdV equation [22] demonstrates the other extreme situation. The sole nonlinearity in the KSE is the convective term, which is also known as “eikonal” nonlinearity [10, 18] in the framework of deriving the eq. 1.

Over the years, a large numbers of numerical studies have been devoted to the KSE; readers are referred to the review paper [18] where a study consists of thorough investigation of different regimes is presented. Among the earlier works, two numerical studies are worth mentioning – one by Frisch et al. [15] where a detailed multiple-scale analysis of the KSE with 2π -periodic boundary conditions is presented, and the other by Christov and Bekyarov [11] where a new Fourier-Galerkin method with a complete orthonormal system of functions in $L^2(-\infty, \infty)$ is applied to the solitary wave problem for the KSE. At about the same time (1992 onwards) attention has also been focused on developing theoretically sound space and time discretization. In [1], Akrivis applied a finite difference scheme to the Eq. 1 with periodic boundary condition. Akrivis also reported in [2] a consistent numerical approach to solve the KSE by employing a finite element Galerkin method with extrapolated Crank-Nicolson scheme. In both cases, rigorous error analysis has been carried out in order to derive refined error bound.

Over the last few decades, a computational approach based on orthogonal spline collocation (OSC) method while seeking numerical solution to the KSE has turned out to be quite popular. It was Manickam et al. [28] who first attempted to solve the KSE by using the orthogonal cubic spline collocation method in conjunction with a second-order splitting method. Later, different types of OSC methods, such as quintic B-Spline collocation (QBSC) method [29], Septic B-spline collocation (SBSC) method [42] have been successfully implemented to seek numerical solution to the KSE. Furthermore, a numerical scheme based on the B-spline functions is introduced in [26] for solving the generalized Kuramoto-Sivashinsky equation (gKSE) where one test example is devoted to discussing the nonlinear stability with convergence for eq. 1 subjected to Gaussian initial condition.

In addition, numerous other methods including discontinuous Galerkin method [41], implicit-explicit BDF method [3], radial basis function (RBF) based mesh-free method [40], etc. have been proposed to find the numerical solutions of the KSE. In another study [32] reported very lately, a lattice Boltzmann model for the KSE is modified to achieve an enhanced level of accuracy and stability. Here model’s enhanced stability enables one to use larger time increments which is more than enough to compensate the extra computational cost due to high lattice speeds – a substantial improvement over the existing model. Another lattice Boltzmann model (LBM) with the Chapman-Enskog expansion has been proposed for the gKSE in [25] where numerically obtained results are found to be in good agreement with the analytical results. The gKSE is also studied with the aid of Chebyshev spectral collocation methods in [21] where the resultant reduced system of ordinary differential equations has been solved by employing the implicit-explicit BDF method depicted in [3]. Very recently, Wade et al. [31] have numerically studied the KSE equation with an additional term representing the dispersive term, arising in turbulent gas flow over laminar liquid.

In this manuscript, numerical solution of the KSE by using the fourth-order Runge-Kutta based implicit-explicit scheme in time along with compact fourth-order finite difference scheme in space is proposed. The proposed scheme takes full benefit of MOL and partial fraction decomposition techniques, therefore it just need to solve two backward Euler-type linear systems at each time step to get the solution. In addition, for the efficient implementation of the scheme it just requires to compute two LU decompositions outside the time loop. Several numerical experiments on the KSE were run in order to study an empirical convergence analysis the accuracy of the proposed scheme with other existing schemes. The numerical results exhibit that the proposed scheme provides better accuracy in most of the cases than the existing schemes considered in this manuscript.

The remainder of the paper is organized as follows. In section 2 compact fourth-order schemes are described to approximate u_x , u_{xx} and u_{xxxx} . In the section 3 the fourth-order Runge-Kutta based implicit-explicit scheme is briefly explained. The linear truncation error and stability analysis of the proposed scheme are discussed in section 4. In section 5, numerical experiments are performed on KSE to test the accuracy and reliability of the proposed scheme. The conclusions are presented in section 6.

2 Fourth-order compact finite differencing schemes

In order to approximate spatial derivatives in KSE, we partitioned the computational domain $\Omega \times [0, T] = \{(x, t) | a \leq x \leq b, 0 \leq t \leq T\}$ into uniform grids described by the set of nodes $\{(x_i, t_j)\}$, in which $x_i = a + (i - 1)h$, $i = 1, \dots, N + 1$, $h = \frac{(b-a)}{N}$, $t_j = jk$, $j = 0, 1, \dots, M$, and $k = \frac{T}{M}$, where h and k are spatial and temporal step sizes, respectively.

There are several methods which are used to generate compact finite difference formula to approximate first, second and fourth-order spatial derivatives. Readers are referred to [27] and references there in for more details on how to

generate compact finite difference formula (CFDF). In this study, the spatial derivatives in KSE are approximated by utilizing the following CFDF:

2.1 Approximation of the first derivative with periodic boundary conditions

If u'_i represents an approximation of the first derivative of $u(x)$ at x_i then an approximation of first derivative may be written as:

$$u'_{i-1} + 4u'_i + u'_{i+1} = \frac{3}{h}(u_{i+1} - u_{i-1}), \quad i = 1, \dots, N, \quad (2)$$

The truncation error for formula 2 is $\mathcal{O}(h^4)$.

The matrix representation of the scheme 2 is given as:

$$L_1 \mathbf{U}' = M_1 \mathbf{U}, \quad (3)$$

where

$$L_1 = \begin{bmatrix} 4 & 1 & 0 & \cdots & 1 \\ 1 & 4 & 1 & \vdots & 0 \\ 0 & \ddots & \ddots & \ddots & 0 \\ \vdots & & 1 & 4 & 1 \\ 1 & \cdots & 0 & 1 & 4 \end{bmatrix}_{N \times N}, \quad M_1 = \frac{3}{h} \begin{bmatrix} 0 & 1 & 0 & \cdots & -1 \\ -1 & 0 & 1 & \vdots & 0 \\ 0 & \ddots & \ddots & \ddots & 0 \\ \vdots & & -1 & 0 & 1 \\ 1 & \cdots & 0 & -1 & 0 \end{bmatrix}_{N \times N}, \quad \mathbf{U} = \begin{bmatrix} u_1 \\ u_2 \\ \vdots \\ u_{N-1} \\ u_N \end{bmatrix}_{N \times 1}.$$

Hence the fourth-order CFDF with periodic boundary conditions for u_x is given by:

$$\mathbf{U}' = L_1^{-1} M_1 \mathbf{U}. \quad (4)$$

2.2 Approximation of the second derivative with periodic boundary conditions

If u''_i represents an approximation of the second derivative of $u(x)$ at x_i then an approximation of second derivatives of $u(x)$ may be written as:

$$u''_{i-1} + 10u''_i + u''_{i+1} = \frac{12}{h^2}(u_{i-1} - 2u_i + u_{i+1}), \quad i = 1, 2, \dots, N. \quad (5)$$

The matrix representation of the scheme 5 is given as:

$$L_2 \mathbf{U}'' = M_2 \mathbf{U}, \quad (6)$$

where

$$L_2 = \begin{bmatrix} 10 & 1 & 0 & \cdots & 1 \\ 1 & 10 & 1 & \vdots & 0 \\ 0 & \ddots & \ddots & \ddots & 0 \\ \vdots & & 1 & 10 & 1 \\ 1 & \cdots & 0 & 1 & 10 \end{bmatrix}_{N \times N}, \quad M_2 = \frac{12}{h^2} \begin{bmatrix} -2 & 1 & 0 & \cdots & 1 \\ 1 & -2 & 1 & \vdots & 0 \\ 0 & \ddots & \ddots & \ddots & 0 \\ \vdots & & 1 & -2 & 1 \\ 1 & \cdots & 0 & 1 & -2 \end{bmatrix}_{N \times N},$$

Hence the fourth-order CFDF with periodic boundary conditions for u_{xx} is given by:

$$\mathbf{U}'' = L_2^{-1} M_2 \mathbf{U}. \quad (7)$$

2.3 Approximation of the fourth derivative with periodic boundary conditions

If $u^{(iv)}_i$ represents an approximation of the fourth derivative of $u(x)$ at x_i then an approximation of fourth derivative of $u(x)$ may be obtained by replacing \mathbf{U} in 6 by \mathbf{U}'' , that is:

$$L_2 \mathbf{U}^{(iv)} = M_2 \mathbf{U}'',$$

where L_2 and M_2 are coefficient matrices defined above.

Hence the fourth-order CFDF with periodic boundary conditions for u_{xxxx} is given by:

$$\mathbf{U}^{(iv)} = L_2^{-2} M_2^2 \mathbf{U}. \quad (8)$$

2.4 Approximation of first derivative with Dirichlet boundary conditions

In this case, uniform grid $x_i = a + (i - 1)h$, $i = 1, \dots, N$, $h = \frac{(b-a)}{N-1}$ is assumed. The standard compact finite difference formula for first derivatives of $u(x, t)$ at interior points is:

$$u'_{i-1} + 4u'_i + u'_{i+1} = \frac{3}{h}(u_{i+1} - u_{i-1}), \quad i = 2, \dots, N-1, \quad (9)$$

where $u_i \approx u(x_i)$ and $u'_i \approx \frac{du(x_i)}{dx}$. The truncation error for formula 9 is $\mathcal{O}(h^4)$. At boundary, when $i = 1$ use:

$$4u'_1 + 12u'_2 = \frac{3}{h} \left(-\frac{34}{9}u_1 + 2u_2 + 2u_3 - \frac{2}{9}u_4 \right), \quad (10)$$

and when $i = N$, the formula is:

$$4u'_N + 12u'_{N-1} = \frac{3}{h} \left(\frac{34}{9}u_N - 2u_{N-1} - 2u_{N-2} + \frac{2}{9}u_{N-3} \right). \quad (11)$$

The truncation errors in the formula 10 and 11 are $\mathcal{O}(h^4)$.

Writing 9-11 into matrix form as:

$$L_1 \mathbf{U}' = M_1 \mathbf{U}, \quad (12)$$

where

$$L_1 = \begin{bmatrix} 4 & 12 & 0 & \cdots & 0 \\ 1 & 4 & 1 & \vdots & 0 \\ 0 & \ddots & \ddots & \ddots & 0 \\ \vdots & & 1 & 4 & 1 \\ 0 & \cdots & 0 & 12 & 4 \end{bmatrix}_{N \times N}, \quad M_1 = \frac{3}{h} \begin{bmatrix} -\frac{34}{9} & 2 & 2 & -\frac{2}{9} & 0 & \cdots & 0 \\ -1 & 0 & 1 & 0 & 0 & & \vdots \\ 0 & -1 & 0 & 1 & 0 & \ddots & \vdots \\ 0 & 0 & -1 & 0 & 1 & \ddots & 0 \\ \vdots & \vdots & \ddots & \ddots & \ddots & \ddots & \vdots \\ 0 & 0 & 0 & \frac{2}{9} & -2 & -2 & \frac{34}{9} \end{bmatrix}_{N \times N}$$

Hence the fourth-order CFDF with Dirichlet boundary conditions for u_x is given by:

$$\mathbf{U}' = L_1^{-1} M_1 \mathbf{U}. \quad (13)$$

2.5 Approximation of second derivative with Dirichlet boundary conditions

The standard compact finite difference formula for second derivatives of $u(x, t)$ at interior points is:

$$u''_{i-1} + 10u''_i + u''_{i+1} = \frac{12}{h^2}(u_{i-1} - 2u_i + u_{i+1}), \quad i = 2, 3, \dots, N-1, \quad (14)$$

where $u''_i \approx \frac{d^2u(x_i)}{dx^2}$. The truncation error for formula 14 is $\mathcal{O}(h^4)$.

At boundary, when $i = 1$, apply:

$$10u''_1 + 100u''_2 = \frac{12}{h^2} \left(\frac{725}{72}u_1 - \frac{190}{9}u_2 + \frac{145}{12}u_3 - \frac{10}{9}u_4 + \frac{5}{72}u_5 \right), \quad (15)$$

and when $i = N$,

$$10u''_N + 100u''_{N-1} = \frac{12}{h^2} \left(\frac{725}{72}u_N - \frac{190}{9}u_{N-1} + \frac{145}{12}u_{N-2} - \frac{10}{9}u_{N-3} + \frac{5}{72}u_{N-4} \right). \quad (16)$$

The truncation error in both of the formulae is also $\mathcal{O}(h^4)$.

Writing 14-16 in matrix form yields:

$$L_2 \mathbf{U}'' = M_2 \mathbf{U}, \quad (17)$$

where

$$L_2 = \begin{bmatrix} 10 & 100 & 0 & \cdots & 0 \\ 1 & 10 & 1 & \vdots & 0 \\ 0 & \ddots & \ddots & \ddots & 0 \\ \vdots & & & 1 & 10 & 1 \\ 0 & \cdots & 0 & 100 & 10 \end{bmatrix}_{N \times N}, M_2 = \frac{12}{h^2} \begin{bmatrix} \frac{725}{72} & -\frac{190}{9} & \frac{145}{12} & -\frac{10}{9} & \frac{5}{72} & \cdots & 0 \\ 1 & -2 & 1 & 0 & 0 & & \vdots \\ 0 & 1 & -2 & 1 & 0 & \ddots & 0 \\ \vdots & \vdots & \vdots & \vdots & \vdots & \ddots & \vdots \\ \vdots & & 0 & 1 & -2 & 1 & 0 \\ 0 & \cdots & 0 & 0 & 1 & -2 & 1 \\ 0 & \cdots & \frac{5}{72} & -\frac{10}{9} & \frac{145}{12} & -\frac{190}{9} & \frac{725}{72} \end{bmatrix}_{N \times N},$$

Hence the fourth-order CFDF with Dirichlet boundary conditions for u_{xx} is given by:

$$\mathbf{U}'' = L_2^{-1} M_2 \mathbf{U}. \quad (18)$$

2.6 Approximation of the fourth derivative with Dirichlet boundary conditions

If $u_i^{(iv)}$ represents an approximation of the fourth derivative of $u(x)$ at x_i then an approximation of fourth derivative of $u(x)$ may be obtained by replacing U in 17 by U'' , that is:

$$L_2 \mathbf{U}^{(iv)} = M_2 \mathbf{U}'', \quad (19)$$

where L_2 and M_2 are coefficient matrices defined above.

Hence the fourth-order CFDF with Dirichlet boundary conditions for u_{xxxx} is given by:

$$\mathbf{U}^{(iv)} = (L_2^{-1} M_2)^2 \mathbf{U}. \quad (20)$$

3 Fourth-order time stepping scheme

This section presents brief derivation procedure of fourth-order implicit-explicit (IMEX4) scheme based on fourth-order exponential time differencing Runge-Kutta (ETDRK4-B)[23] time integrator to solve following equation with periodic boundary conditions:

$$\frac{\partial u}{\partial t} + \mathcal{L}u = \mathcal{F}(u, t), \quad u(x, 0) = g(x) \quad (21)$$

where \mathcal{L} and \mathcal{F} represent linear and nonlinear operators of KSE, respectively. Approximating $\mathcal{L}u = \alpha u_{xx} + \beta u_{xxxx}$ with schemes 7 and 8 respectively and $\mathcal{F}(u, t)$ with scheme 4, resulted the following system of ODEs:

$$\frac{\partial \mathbf{U}}{\partial t} + L \mathbf{U} = F(\mathbf{U}, t), \quad (22)$$

where $L = L_2^{-2} (\alpha L_2 M_2 + \beta M_2^2)$ and $F(\mathbf{U}, t) = -\frac{1}{2} L_1^{-1} M_1 \mathbf{U}^2$.

Let $k = t_{n+1} - t_n$ be the time step size, then using a variation of constant formula, the following recurrence formula is obtained:

$$\mathbf{U}_{n+1} = e^{-kL} \mathbf{U}_n + k \int_0^1 e^{-kL(1-\tau)} F(\mathbf{U}(t_n + \tau k), t_n + \tau k) d\tau, \quad (23)$$

where $\mathbf{U}_n = \mathbf{U}(t_n)$. The expression 23 is an exact solution of system 22 and approximation of its integral term leads to various ETD schemes. This paper considers a popular ETD scheme of Runge-Kutta type, namely ETDRK4-B [23] and presents its implicit-explicit version for its general applicability.

The ETDRK4-B [23] scheme is given as:

$$\mathbf{U}_{n+1} = \varphi_0(kL) \mathbf{U}_n + k \varphi_1(kL) F_n + k \varphi_2(kL) (-3F_n + 2F_n^a + 2F_n^b - F_n^c) + 4k \varphi_3(kL) (F_n - F_n^a - F_n^b + F_n^c), \quad (24)$$

where

$$\begin{aligned} F_n &= F(\mathbf{U}_n, t_n), \quad F_n^a = F(\mathbf{a}_n, t_n + \frac{k}{2}), \quad F_n^b = F(\mathbf{b}_n, t_n + \frac{k}{2}) \text{ and } F_n^c = F(\mathbf{c}_n, t_n + k), \\ \mathbf{a}_n &= \varphi_0(kL/2)\mathbf{U}_n + \frac{k}{2}\varphi_1(kL/2)F_n, \\ \mathbf{b}_n &= \varphi_0(kL/2)\mathbf{U}_n + \frac{k}{2}\varphi_1(kL/2)F_n + k\varphi_2(kL/2)(F_n^a - F_n), \\ \mathbf{c}_n &= \varphi_0(kL)\mathbf{U}_n + k\varphi_1(kL)F_n + 2k\varphi_2(kL)(F_n^b - F_n). \end{aligned}$$

Note that the scheme 24 contains matrix functions of the form:

$$\varphi_0(kL) = e^{-kL}, \quad \varphi_\mu(kL) = (-kL)^{-\mu} \left(e^{-kL} - \sum_{j=0}^{\mu-1} \frac{(-kL)^j}{j!} \right), \quad \mu = 1, 2, 3. \quad (25)$$

If an eigenvalues of L close to zero, the direct computation of phi functions in 25 is a challenging problem in numerical analysis due to disastrous cancellation error in the computation. To overcome this and other numerical issues associated with it, many researchers have proposed different techniques to compute these phi functions. Some of the well-known techniques include (i) the rational approximation of $\varphi_\mu(kL)$ [7, 8] (ii) the Krylov subspace method [16, 39], and (iii) polynomial approximation of $\varphi_\mu(kL)$ [9, 38].

This study focuses on the rational approximation of $\varphi_\mu(kL)$ and introduces implicit-explicit version of ETD RK4-B schemes utilizing a partial fraction decomposition technique given in [7]. In order to alleviate computational difficulties associated in direct computation of $\varphi_\mu(kL)$, at first a fourth-order (2, 2)-Padé approximation to e^{-kL} is utilized, which helps to avoids direct computation of the matrix exponential and higher powers of matrix inverse. In addition, another advantage we found in utilizing (2, 2)-Padé approximation is that the factors L^{-1} and L^{-3} cancel out in ETD RK4-B scheme.

Implementation of (2, 2)-Padé approximation $R_{2,2}(kL) = (12I + 6kL + k^2L^2)^{-1}(12I - 6kL + k^2L^2)$ into 24 to approximate matrix exponential functions yields:

$$\mathbf{U}_{n+1} = R_{2,2}(kL)\mathbf{U}_n + P_1(kL)F_n + P_2(kL)(-3F_n + 2F_n^a + 2F_n^b - F_n^c) + P_3(kL)(F_n - F_n^a - F_n^b + F_n^c), \quad (26)$$

where

$$\begin{aligned} P_1(kL) &= 12k(12I + 6kL + k^2L^2)^{-1}, \\ P_2(kL) &= k(6I + kL)(12I + 6kL + k^2L^2)^{-1}, \\ P_3(kL) &= 2k(4I + kL)(12I + 6kL + k^2L^2)^{-1}. \end{aligned}$$

In addition:

$$\begin{aligned} \mathbf{a}_n &= \tilde{R}_{2,2}(kL)\mathbf{U}_n + \tilde{P}_1(kL)F_n, \\ \mathbf{b}_n &= \tilde{R}_{2,2}(kL)\mathbf{U}_n + \tilde{P}_1(kL)F_n + \tilde{P}_2(kL)(F_n^a - F_n), \\ \mathbf{c}_n &= R_{2,2}(kL)\mathbf{U}_n + P_1(kL)F_n + 2P_2(kL)(F_n^b - F_n), \end{aligned}$$

with

$$\begin{aligned} \tilde{R}_{2,2}(kL) &= (48I - 12kL + k^2L^2)(48I + 12kL + k^2L^2)^{-1}, \\ \tilde{P}_1(kL) &= 24k(48I + 12kL + k^2L^2)^{-1}, \\ \tilde{P}_2(kL) &= 2k(12I + kL)(48I + 12kL + k^2L^2)^{-1}. \end{aligned}$$

3.1 Fourth-order implicit-explicit Runge-Kutta type scheme

Since the scheme 26 consists of high order matrix polynomials to invert, the direct implementation of it would be computationally burdensome and numerically unstable, if the matrices have high condition numbers. In addition, round off error in computing the power of the matrices can produce bad approximations [30]. In order to handle this difficulty, $R_{2,2}(kL)$ and $\tilde{R}_{2,2}(kL)$ will not be computed directly. Instead, the problem of stably computing the inverse of matrix polynomials inherent in 26 is handled by utilizing a partial fraction decomposition technique as suggested in [7]. This

decomposition does reduce the computational complexity to just two LU decompositions over the entire time interval (provided the space step h , and time step k are held constant). In addition, this decomposition approach is important in alleviating ill-conditioning problems because only implicit Euler type solvers are required. A description of the scheme after implementing a partial fraction decomposition technique is presented in the following algorithm and from this point the algorithm is referenced with IMEXRK4 scheme.

Algorithm 1 IMEXRK4 scheme

Step 1:

Solve the linear system $(kL - \tilde{c}_1 I)R_a = \tilde{w}_1 \mathbf{U}_n + k\tilde{\Omega}_1 F_n$.

Define $\mathbf{a}_n = \mathbf{U}_n + 2 \operatorname{Re}(R_a)$,

and $F_n^{\mathbf{a}} = F(\mathbf{a}_n, t_n + \frac{k}{2})$.

Step 2:

Solve the linear system $(kL - \tilde{c}_1 I)R_b = \tilde{w}_1 \mathbf{U}_n + k(\tilde{\Omega}_1 - \tilde{\Omega}_2) F_n + k\tilde{\Omega}_2 F_n^{\mathbf{a}}$,

Define $\mathbf{b}_n = \mathbf{U}_n + 2 \operatorname{Re}(R_b)$,

and $F_n^{\mathbf{b}} = F(\mathbf{b}_n, t_n + \frac{k}{2})$.

Step 3:

Solve the linear system $(kL - c_1 I)R_c = w_1 \mathbf{U}_n + k(w_{11} - 2w_{21}) F_n + 2kw_{21} F_n^{\mathbf{b}}$,

Define $\mathbf{c}_n = \mathbf{U}_n + 2 \operatorname{Re}(R_c)$,

and $F_n^{\mathbf{c}} = F(\mathbf{c}_n, t_n + k)$.

Step 4:

Solve the linear system $(kL - c_1 I)R_u = w_1 \mathbf{U}_n + k(w_{11} - 3w_{21} + w_{31}) F_n + k(2w_{21} - w_{31})(F_n^{\mathbf{a}} + F_n^{\mathbf{b}}) - k(w_{21} - w_{31}) F_n^{\mathbf{c}}$.

Evaluate $\mathbf{U}_{n+1} = \mathbf{U}_n + 2 \operatorname{Re}(R_u)$,

In order to implement this IMEXRK4 scheme, poles and corresponding weights were computed for $R_{2,2}(kL)$, $\{P_i(kL)\}_{i=1}^3$, $\tilde{R}_{2,2}(kL)$, and $\{\tilde{P}_i(kL)\}_{i=1}^2$ using Maple, which are as follows:

$$\begin{aligned} c_1 &= -3.0 + i1.7320508075688772935, & w_1 &= -6.0 - i10.39230484541326376, \\ w_{11} &= -i3.4641016151377545871, & w_{21} &= 0.5 - i0.8660254037844386467, \\ w_{31} &= 1.0 - i0.57735026918962576452, & \tilde{c}_1 &= -6.0 + i3.4641016151377545871, \\ \tilde{w}_1 &= -12.0 - i20.784609690826527522, & \tilde{\Omega}_1 &= -i3.4641016151377545870, \\ \tilde{\Omega}_2 &= 1.0 - i1.7320508075688772935. \end{aligned}$$

4 Linear analysis

The linear truncation error and stability analysis of the scheme 26 are presented in this section.

4.1 Truncation error analysis

It is obvious that the overall spatial discretization is of order four because a fourth-order CFDF is applied to linear parts of the KSE. To analyze the overall local temporal truncation error of the scheme 26 for KSE, the following linear semi-discretization system is considered:

$$\frac{\partial \mathbf{U}}{\partial t} = -L\mathbf{U} + R\mathbf{U}, \tag{27}$$

where L may represent matrices derived from the linear spatial discretization of second and fourth-order spatial derivatives, R represents linear spatial discretization of first-order derivative term of a linear KSE respectively, and \mathbf{U} is a vector of unknowns.

Applying scheme 26 to Eq. 27 yields:

$$\mathbf{U}_{n+1} = \left(I + \frac{kL}{2} + \frac{k^2L^2}{12}\right)^{-1} \left(\left(I - \frac{kL}{2} + \frac{k^2L^2}{12} + Rk\right)\mathbf{U}_n + \frac{Rk}{2} \left(I + \frac{kL}{6}\right) (-3 + 2\mathbf{a}_n + 2\mathbf{b}_n - \mathbf{c}_n) + \frac{2Rk}{3} \left(I + \frac{kL}{4}\right) (1 - \mathbf{a}_n - \mathbf{b}_n + \mathbf{c}_n) \right), \quad (28)$$

where

$$\begin{aligned} \mathbf{a}_n &= \left(I + \frac{1}{4}kL + \frac{1}{48}k^2L^2\right)^{-1} \left(I - \frac{1}{4}kL + \frac{1}{48}k^2L^2 + \frac{1}{2}Rk\right)\mathbf{U}_n, \\ \mathbf{b}_n &= \left(I + \frac{1}{4}kL + \frac{1}{48}k^2L^2\right)^{-1} \left(\left(I - \frac{1}{4}kL + \frac{1}{48}k^2L^2 + \frac{1}{2}Rk\right)\mathbf{U}_n + \frac{1}{2}Rk \left(I + \frac{1}{12}kL\right) (\mathbf{a}_n - \mathbf{U}_n) \right), \\ \mathbf{c}_n &= \left(I + \frac{1}{2}kL + \frac{1}{12}k^2L^2\right)^{-1} \left(\left(I - \frac{1}{2}kL + \frac{1}{12}k^2L^2 + Rk\right)\mathbf{U}_n + Rk \left(I + \frac{1}{6}kL\right) (\mathbf{b}_n - \mathbf{U}_n) \right). \end{aligned}$$

Taylor expansion of Eq. 28 yields:

$$\begin{aligned} \mathbf{U}_{n+1} &= \left(I + (R-L)k + \left(\frac{L^2}{2} - LR + \frac{R^2}{2}\right)k^2 + \left(\frac{L^2R}{2} - \frac{LR^2}{2} - \frac{L^3}{6} + \frac{R^3}{6}\right)k^3 + \right. \\ &\quad \left. \left(\frac{L^4}{24} + \frac{L^2R^2}{4} - \frac{LR^3}{6} - \frac{L^3R}{6} + \frac{R^4}{24}\right)k^4 + \dots \right) \mathbf{U}_n. \end{aligned} \quad (29)$$

Since the exact solution of Eq. 27 is:

$$\mathbf{U}(t_{n+1}) = e^{(R-L)k} \mathbf{U}(t_n).$$

Then the local truncation error of the scheme 26 is:

$$\begin{aligned} \mathbf{e}_{n+1} &= \left(I + (R-L)k + \left(\frac{L^2}{2} - RL + \frac{R^2}{2}\right)k^2 + \left(\frac{RL^2}{2} - \frac{LR^2}{2} - \frac{L^3}{6} + \frac{R^3}{6}\right)k^3 + \right. \\ &\quad \left. \left(\frac{L^4}{24} + \frac{L^2R^2}{4} - \frac{LR^3}{6} - \frac{L^3R}{6} + \frac{R^4}{24}\right)k^4 + \dots \right) \mathbf{U}_n - e^{(R-L)k} \mathbf{U}(t_n) = \mathcal{O}(k^5). \end{aligned} \quad (30)$$

Hence the scheme 26 is fourth-order in time discretization.

4.2 Stability analysis

The linear stability of the scheme 26 was analyzed by plotting its stability regions (see in [6] and references therein) for the non-linear autonomous ODE:

$$u_t = -cu + F(u), \quad (31)$$

where $F(u)$ is a nonlinear part and c represents the approximation of the linear parts of KSE. Let us assume that there exists a fixed point u_0 such that $-cu_0 + F(u_0) = 0$. Linearizing about this fixed point, we thus obtain:

$$u_t = -cu + \gamma u, \quad (32)$$

where u is perturbation of u_0 , and $\gamma = F'(u_0)$. If 31 represents a system of ODEs, then γ is a diagonal or a block diagonal matrix containing the eigenvalues of F . To keep the fixed point stable, we need that $\text{Re}(\gamma - c) < 0$, for all γ (see[13]). This approach only provides an indication to how stable a numerical method is, since in general one cannot linearize both terms simultaneously [23].

In general, the parameters c and γ may both be complex-valued. The stability region of the scheme 26 is four dimensional and therefore difficult to represent [13]. The two-dimensional stability region is obtained, if both c and γ are purely imaginary or purely real [14], or if γ is complex and c is fixed and real [6].

Utilization of the scheme 26 to the linearized Eq. 32 leads to a recurrence relation involving u_n , and u_{n+1} . By letting $r = \frac{u_{n+1}}{u_n}$, $x = \gamma k$, and $y = -ck$, we come up with the following amplification factor:

$$r(x, y) = c_0 + c_1x + c_2x^2 + c_3x^3 + c_4x^4, \quad (33)$$

where

$$\begin{aligned}
 c_0 &= 1 + y + \frac{1}{2}y^2 + \frac{1}{6}y^3 + \frac{1}{24}y^4 + \frac{1}{144}y^5 + O(y^6), \\
 c_1 &= 1 + y + \frac{1}{2}y^2 + \frac{1}{6}y^3 + \frac{7}{192}y^4 + \frac{5}{2304}y^5 + O(y^6), \\
 c_2 &= \frac{1}{2} + \frac{1}{2}y + \frac{1}{4}y^2 + \frac{23}{288}y^3 + \frac{11}{768}y^4 - \frac{37}{27648}y^5 + O(y^6), \\
 c_3 &= \frac{1}{6} + \frac{1}{6}y + \frac{47}{576}y^2 + \frac{77}{3456}y^3 + \frac{5}{9216}y^4 - \frac{515}{165888}y^5 + O(y^6), \\
 c_4 &= \frac{1}{24} + \frac{1}{32}y + \frac{35}{3456}y^2 - \frac{1}{13824}y^3 - \frac{169}{82944}y^4 - \frac{457}{331776}y^5 + O(y^6).
 \end{aligned}$$

The boundaries of the stability regions of the scheme 26 are obtained by substituting $r = e^{i\theta}$, $\theta \in [0, 2\pi]$ into the Eq. 33 and solving for x , but unfortunately we do not know the explicit expression for $|r(x, y)| = 1$. We will only be able to plot it and in this paper we have plotted the stability regions for the two cases. At first, this study focuses on the case where γ is complex and c is fixed and real. The analysis begins by selecting several real negative values of y and looking for a region of stability in the complex x plane where $|r(x, y)| = 1$. The corresponding families of stability regions of the scheme 26 in the complex x plane are plotted in Fig. 1. According to Beylkin et al. [6] for scheme to be applicable, it is important that stability regions grow as $y \rightarrow -\infty$. As we can see in Fig. 1, the stability regions grow larger as $y \rightarrow -\infty$. These regions give an indication of the stability of the proposed scheme.

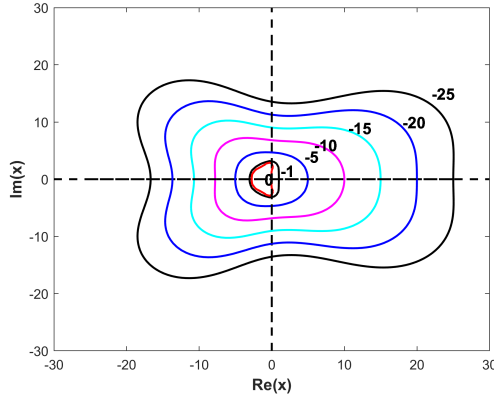


Figure 1: Stability regions for different values of $y \in \mathbb{R}^-$

In the second case, we assume γ is complex and c is purely imaginary and stability regions for different values of $y = -5i, 5i, -20i$, and $20i$ are depicted in Fig. 2 (a)-(d).

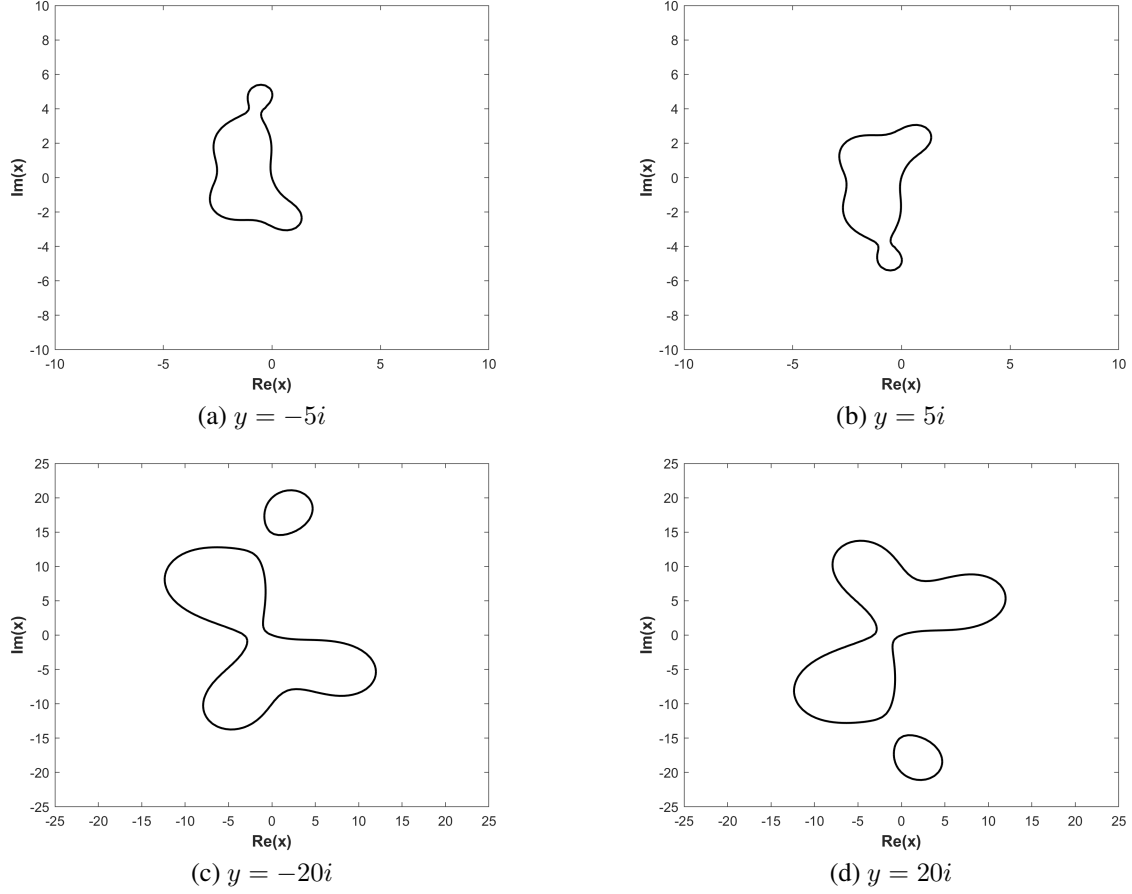


Figure 2: Stability regions for different values of $y = -5i, 5i, -20i$, and $20i$

5 Numerical experiments and discussions

In this section, we present the results of extensive numerical experiments carried out by implementation of the proposed scheme on four test problems in order to demonstrate the efficiency and accuracy of the scheme. All the numerical experiments are conducted in MATLAB 9.3 platforms based on an Intel Core i52410M 2.30 GHz workstation. The accuracy of the schemes is measured in terms of maximum norm errors $\|\cdot\|_\infty$ and global relative error (GRE) at the final time $t = T$ which are defined as:

$$\|\cdot\|_\infty = \max_{1 \leq i \leq N} |u(x_i, T) - U_i^M|,$$

$$\text{GRE} = \frac{\sum_i |u(x_i, T) - U_i^M|}{\sum_i |u(x_i, T)|},$$

where u , and U are the exact and numerical solutions, respectively.

When the exact solution of the considered problem(s) is/are available, we compute the spatial convergence rate with:

$$\text{order} = \frac{\log_{10}(\|u - U_h\|_\infty / \|u - U_{h/2}\|_\infty)}{\log_{10}(2)}$$

and the temporal convergence rate with:

$$\text{order} = \frac{\log_{10}(\|u - U_k\|_\infty / \|u - U_{k/2}\|_\infty)}{\log_{10}(2)}$$

where $\|u - U_h\|_\infty$ and $\|u - U_{h/2}\|_\infty$ are maximum error norms with spatial step sizes equal to h and $\frac{h}{2}$, respectively. Similar description is valid for temporal convergence rate.

On the other hand, when the exact solution of the problem(s) is/are unavailable, we utilize

$$\text{order} = \frac{\log_{10}(E_k/E_{\frac{k}{2}})}{\log_{10}(2)}, \quad (34)$$

where $E_k = \|U_k - U_{2k}\|_\infty$ and $E_{\frac{k}{2}} = \|U_{\frac{k}{2}} - U_k\|_\infty$ are maximum norm errors at k and $\frac{k}{2}$ to measure the temporal convergence rate of the scheme.

Example 1 (Benchmark Problem): In this example, the Kuramoto-Sivashinsky with $\alpha = -1$ and $\beta = 1$ over a domain $\Omega = [-50, 50]$, with the analytical solution

$$u(x, t) = \mu + \frac{15 \tanh^3(\nu(x - \mu t - x_0)) - 45 \tanh(\nu(x - \mu t - x_0))}{19^{\frac{3}{2}}} \quad (35)$$

is considered.

The initial and boundary conditions are extracted from the exact solution 35. This example is considered as a benchmark problem in order to investigate the performance in terms of accuracy and efficiency of the proposed method. The parameters in 35 are chosen as $\mu = 5$, $\nu = \frac{1}{2\sqrt{19}}$ and $x_0 = -25$.

In order to investigate the order of accuracy and computational efficiency of the proposed scheme IMEXRK4 for solving KSE, a numerical test on Example 1 was performed. In the computation, a simulation was run up to $t = 2.0$ by initially setting $h = 4$ and $k = 0.025$ then reduced both of them by a factor of 2 in each refinement. The maximum error and rates of convergence are listed in Table 1. As can be seen from Table 1 that the computed convergence rates of the proposed schemes apparently demonstrate the expected fourth-order accuracy in both time and space.

Table 1: The maximum error, rates of convergence, and CPU time of IMEXRK4 for Example 1 at $t = 2.0$

h & k	4 & 0.025	2 & 0.0125	1 & 0.00625	0.5 & 0.003125
$\ \cdot\ _\infty$	6.157E-03	3.775E-04	2.396E-05	1.461E-06
Order	-	4.0278	3.9777	4.0359
CPU(s)	0.2004	0.5011	1.6728	8.0996

In order to visualize the space and time rates of convergence of the proposed scheme, we illustrated them in Fig. 3 with log-log scale graph. From Fig. 3, it can be seen that the slopes of the regression line for maximum errors both in time and spatial directions are close to four, which corresponds to the fourth-order scheme both in time and space.

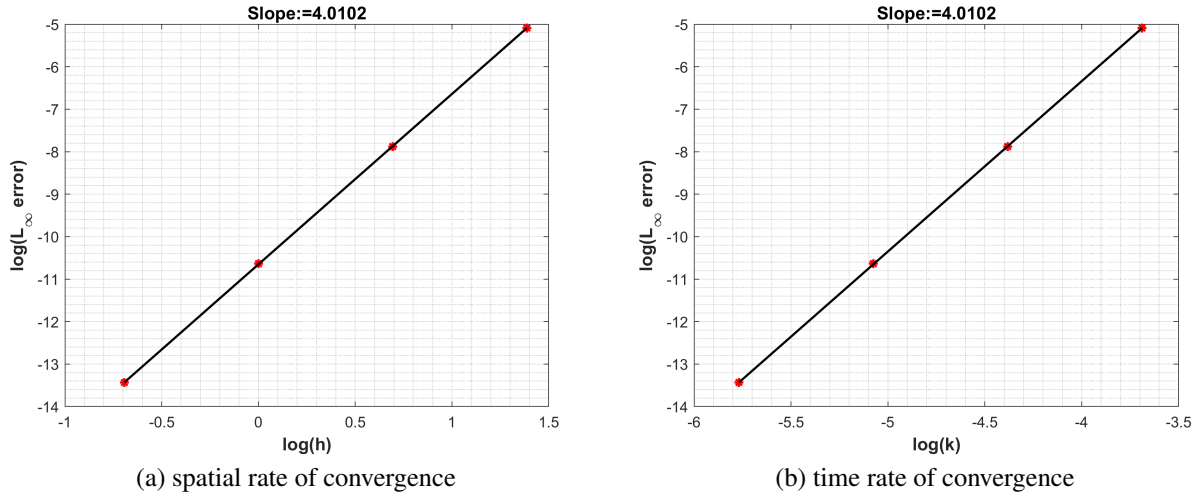


Figure 3: Log-log plots of spatial and time rates of convergence of the proposed method.

We ran another sets of experiment in Example 1 with $h = 0.5, k = 0.01$ until time $t = 10$ and captured the 3D view of the solution profile in Fig. 4 (a). From Fig. 4 (a)-(b), we can see the the solution obtained via using the proposed scheme is close to the exact solution.

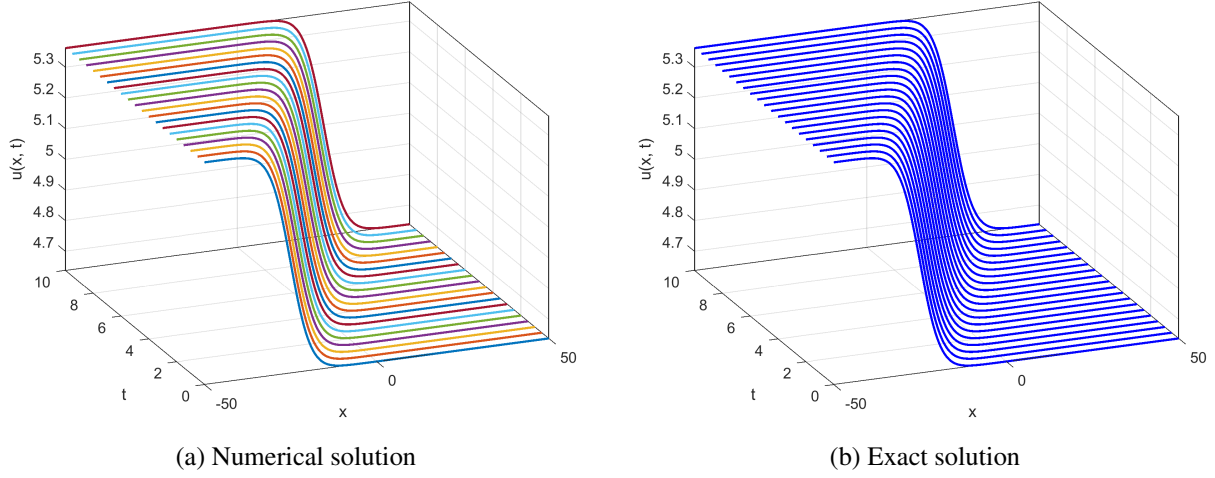


Figure 4: Numerical solution vs exact solution for various time $t \in [0, 10]$.

In Table 2, we compare the scheme IMEXRK4 with earlier schemes: SBSC[42], QBSC[29], and LBM[25] by listing GRE of $u(x, t)$ with $N = 200, k = 0.01$ at different time levels $t \leq 12$. Table 2 clearly indicates that the numerical results obtained via proposed scheme are more accurate than that obtained via SBSC[42], QBSC[29] and LBM[25].

Table 2: Comparison of GRE at different time with $N = 200$ and $k = 0.01$ for Example 1.

IMEXRK4	Time(t)	6	8	10	12
	GRE	7.624E-08	8.092E-08	8.589E-08	3.188E-07
SBSC	Time(t)	6	8	10	12
	GRE	1.625E-07	1.940E-07	2.229E-07	5.314E-07
QBSC	Time(t)	6	8	10	12
	GRE	6.509E-06	7.132E-06	7.310E-06	8.776E-06
LBM	Time(t)	6	8	10	12
	GRE	7.881E-06	9.532E-06	1.089E-05	1.179E-05

Example 2 (KSE with periodic boundary conditions): In this example, we consider the KSE with $\alpha = 1$ and $\beta = 1$ over a domain $\Omega = [0, 32\pi]$ along with periodic boundary conditions and following initial condition:

$$u(x, 0) = \cos\left(\frac{x}{16}\right)\left(1 + \sin\left(\frac{x}{16}\right)\right). \quad (36)$$

Two sets of numerical experiments on Example 2 were conducted. In the first sets of the experiment, the order of accuracy in the temporal direction of the proposed method with periodic boundary conditions was checked by running an experiment until time $T = 10.0$ with $N = 256$. Initially, $k = \frac{1}{2}$ was set and repeatedly halved it at each time and numerical results are captured in Table 3. The error values E_k listed for IMEXRK4 scheme in Table 3 are again calculated through a maximal difference between each simulation. From Table 3, it can be seen that the proposed scheme is able to achieve the expected fourth-order accuracy in time with periodic boundary conditions.

Table 3: The maximum error, time rates of convergence, and CPU time of IMEXRK4 for Example 2 with $N = 256$ at $t = 10.0$

k	1/4	1/8	1/16	1/32
E_k	9.031E-04	6.291E-05	3.922E-06	2.442E-07
Order	-	3.8436	4.0034	4.0052
CPU(s)	1.1791	2.1269	3.3537	5.2132

To better understand the applicability of the IMEXRK4 scheme to simulate the long time behavior of the KSE, a second sets of experiment was conducted on Example 2 until the long time $t = 150$ with $N = 256$, $k = \frac{1}{4}$ and $t = 300$ with $N = 512$, $k = \frac{1}{8}$. The chaotic solution profiles of the component $u(x, t)$ for $t \in [0, 150]$ and for $t \in [0, 300]$ were captured in Fig. 5 (a) and (b) respectively. Chaotic solution profile corresponds for $t \leq 150$ in the Fig. 5 (a) are in good agreement with the results depicted in [20] – therefore, we are confident that the profile corresponds for $t \leq 300$ is correct and reliable.

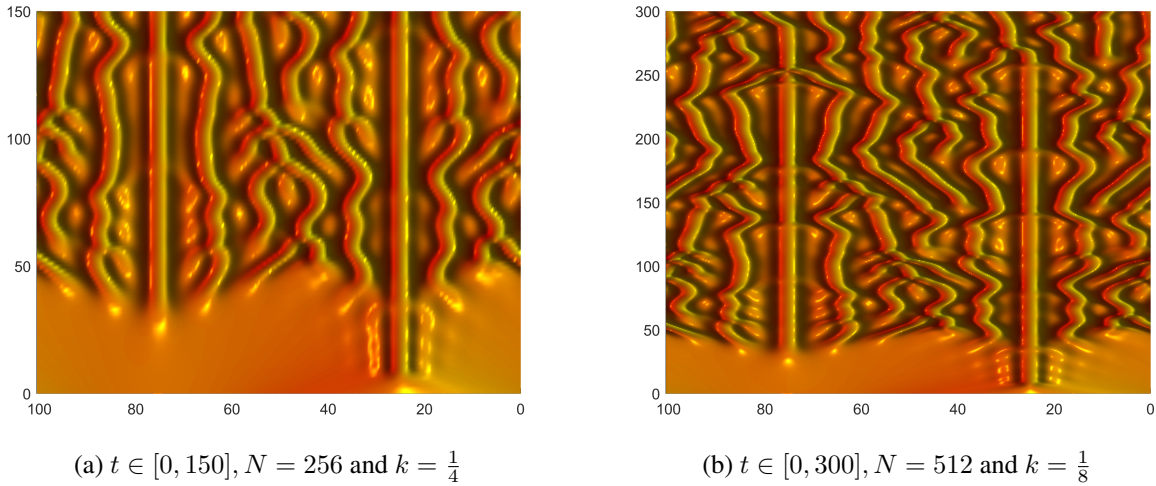


Figure 5: Chaotic solution profile of the component $u(x, t)$ at various time obtained via IMEXRK4.

Example 3 (KSE with Gaussian initial condition): Here, we consider the KSE with $\alpha = 1$ and $\beta = 1$ which exhibits chaotic behavior over a finite domain $\Omega = [-30, 30]$ with homogeneous Dirichlet boundary conditions and the following Gaussian initial condition

$$u(x, 0) = \exp(-x^2). \quad (37)$$

In what follows, again on Example 3 two sets of numerical experiments were performed. In the first sets of the experiment, the order of accuracy in the temporal direction of the proposed scheme with homogeneous Dirichlet boundary conditions was examined by running an experiment until time $T = 1.0$ with fixed $N = 101$. Again the error values reported in Table 4 are calculated through a maximal difference between each simulation which is obtained by repeatedly halving an initial time step size $k = \frac{1}{2}$ at each time. From the results, it can be seen that the proposed scheme is able to achieve the expected fourth-order accuracy in time.

Table 4: The maximum error, time rates of convergence, and CPU time of IMEXRK4 for Example 3 with $N = 101$ at $t = 1$.

k	0.01/2	0.01/4	0.01/8	0.01/16
E_k	2.723E-08	1.976E-09	1.324E-10	8.613E-12
Order	-	3.7847	3.8995	3.9422
CPU(s)	0.5543	1.0044	1.9298	3.4635

In the second sets of experiment, the chaotic behavior of the component $u(x, t)$ is simulated for Gaussian initial condition. The simulations are accomplished in $t \in [0, 30]$ with the parameters $N = 101$ and $k = 0.1$ and captured in Fig. 6 with aerial and 3D views. From Fig. 6, we can see clearly that the result shows same behavior as reported in [26, 29].

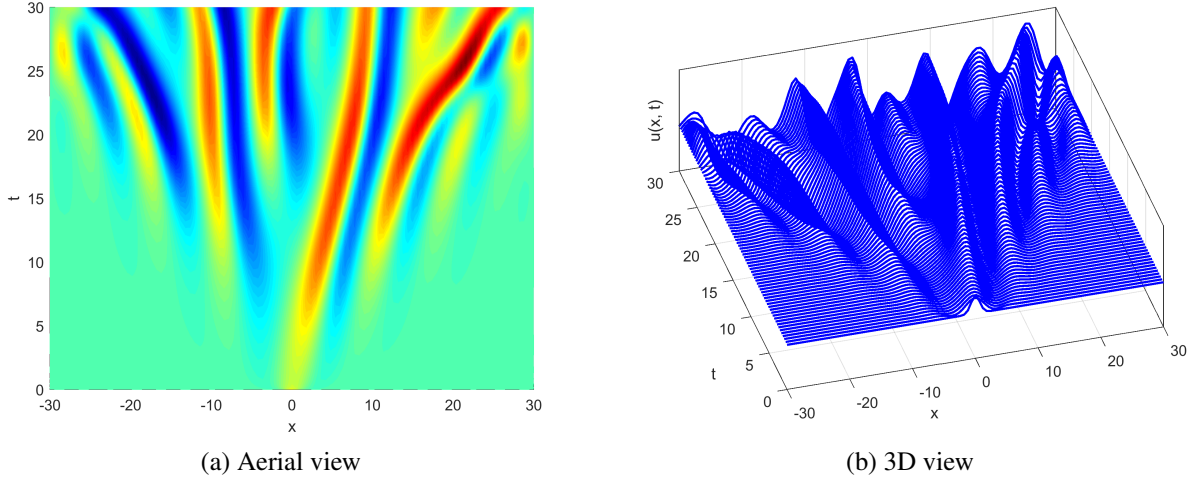


Figure 6: The aerial and 3D chaotic solution profile of the KSE with $N = 101$, $k = 0.1$ at $t \in [0, 30]$ for Example 3.

Example 4 (KSE with different values of β): The KSE with $\alpha = 1$ and different values of β over a finite domain $\Omega = [-1, 1]$ along with homogeneous Dirichlet boundary conditions and the following initial condition is considered here:

$$u(x, 0) = -\sin(\pi x). \quad (38)$$

For the empirical convergence analysis in the temporal direction of the proposed scheme, we ran an experiment until time $T = 1.0$ with $\beta = 1.1$ and fixed $h = 0.05$. The error values reported in Table 5 are computed through a maximal difference between each simulation which is obtained by repeatedly halving an initial time step size $k = 0.005$ at each time. From the results, it can be seen that the proposed scheme is able to exhibit the expected fourth-order accuracy in time.

Table 5: The maximum error, time rates of convergence, and CPU time of IMEXRK4 for Example 4 with $\beta = 1.1$, $h = 0.05$ at $t = 1$.

k	0.005/2	0.005/4	0.005/8	0.005/16
E_k	1.431E-08	9.7926E-10	6.532E-11	3.320E-12
Order	-	3.8692	3.9060	4.2983
CPU(s)	1.0360	2.1329	3.7341	5.6047

The space-time evolution profile of $u(x, t)$ via IMEXRK4 scheme with different values of β , $h = 0.05$, $k = 0.001$ at different time levels were depicted in Fig. 7. The results in Fig. 7 clearly exhibit good agreement with results reported in [29, 28].

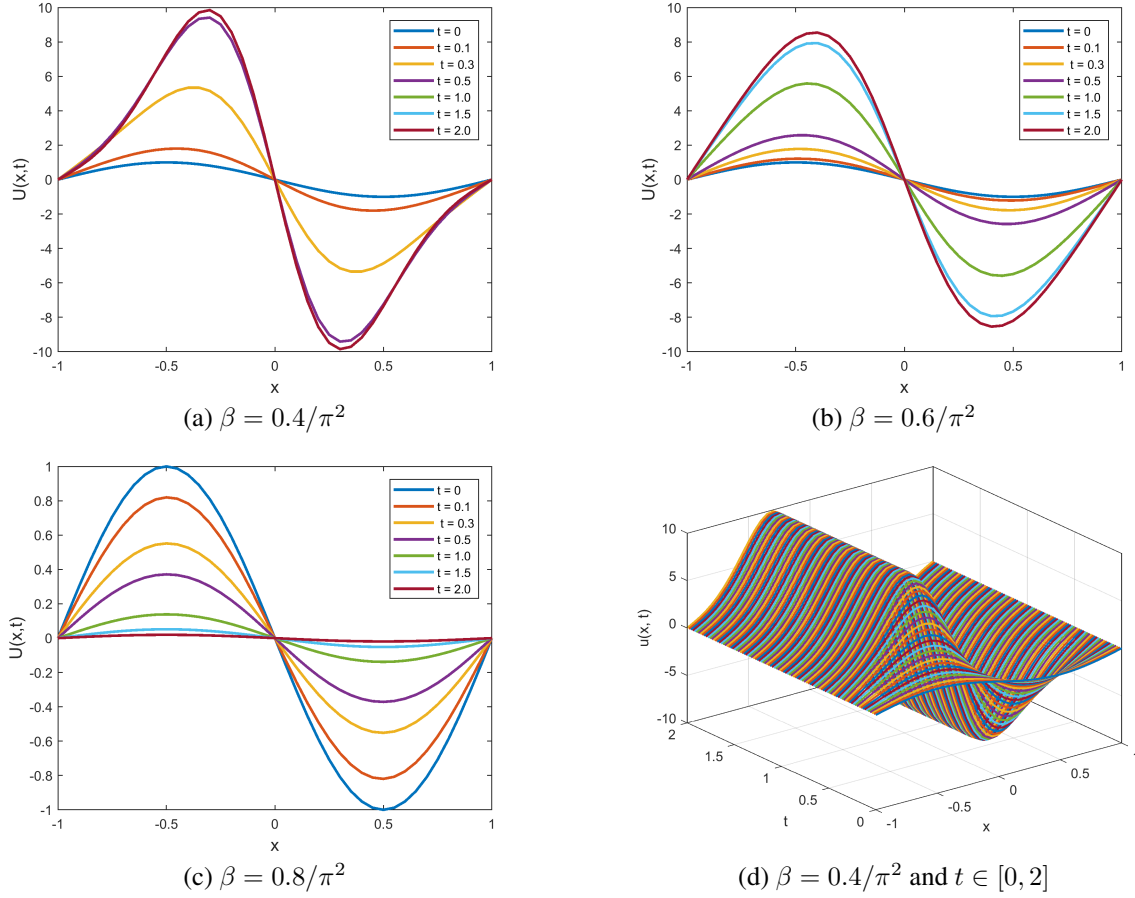


Figure 7: Space-time evolution profile of the component $u(x, t)$ obtained via IMEXRK4 scheme with various values of β at different time levels.

6 Conclusions

This manuscript introduced a fourth-order scheme both in time and space to solve the KSE. The proposed method utilized a compact fourth-order finite difference scheme for a spatial discretization and the fourth-order Runge-Kutta based implicit-explicit scheme for time discretization. A Compact finite difference scheme is used to transform the KSE to a system of ordinary differential equations (ODEs) in time, and then, fourth-order time integrator is implemented to solve the resulting ODEs. Calculation of local truncation error and an empirical convergence analysis exhibited the fourth-order accuracy of the proposed scheme. The performance and applicability of the scheme have been investigated by testing it on several test problems. The computed numerical solutions maintain a good accuracy compared with the exact solution. In addition, the numerical results exhibited that the proposed scheme provides better accuracy in comparison with other existing schemes.

References

- [1] G. D. Akrivis, Finite difference discretization of the Kuramoto-Sivashinsky equation, *Numer. Math.* 63 (1992) 1-11.
- [2] G. D. Akrivis, Finite element discretization of the Kuramoto-Sivashinsky equation, *Numer. Analysis and Mathematical Modeling* 29 (1994) 155-163.
- [3] G. Akrivis, Y-S Smyrlis, Implicit-explicit BDF methods for the Kuramoto-Sivashinsky equation, *Appl. Numer. Math.* 51 (2004) 159-161.
- [4] S. V. Alekseenko, V. E. Nakoryakov, B. G. Pokusaev, Wave formation on vertical falling liquid films, *Internat. J. Multiphase Flow*. 11 (1985) 607-627.

- [5] D. J. Benny, Long waves in liquid film, *J. Maths & Phys.* 45 (1966) 150-155.
- [6] G. Beylkin, J.M. Keiser, L. Vozovoi, A new class of time discretization schemes for the solution of nonlinear PDEs, *J. Comp. Phys.* 147 (1998) 362-387.
- [7] H. P. Bhatt, A. Q. M. Khaliq, Higher order exponential time differencing scheme for system of coupled nonlinear Schrödinger equations, *Appl. Math. Comput.* 228(2014) 271-291.
- [8] H. P. Bhatt, A. Q. M. Khaliq, The locally extrapolated exponential time differencing LOD scheme for multidimensional reaction-diffusion systems, *J. Comput. Appl. Math.* 285 (2015) 256-278.
- [9] M. Caliarì, A. Ostermann, Implementation of exponential Rosenbrock type integrals, *App. Numer. Math.* 59 (2009) 568-581.
- [10] C. I. Christov, M. G. Velarde, Dissipative Solitons, *Physica D.* 86 (1995) 323-347.
- [11] C. I. Christov, K. L. Bekyarov, A Fourier-series method for solving soliton problems, *SIAM J. Sci. Stat. Comp.* 11(4) (1990) 631-647.
- [12] P. Clavin, Dynamic behavior of premixed flame fronts in laminar and turbulent flows, *Prog. Energy Combustion Sci.* 11(1) (1985) 1-59.
- [13] S. M. Cox, and P. C. Matthews, Exponential time differencing for stiff systems, *J. Comp. Phys.* 176 (2002) 430-455.
- [14] B. Fornberg, T. A. Driscoll, A fast spectral for nonlinear wave equations with linear dispersion, *J. Comp. Phys.* 155 (1999) 456-467. 937-954.
- [15] U. Frisch, Z. S. She, O. Thual, Viscoelastic behaviour of cellular solutions to the Kuramoto-Sivashinsky model, *J. Fluid. Mech.* 168 (1986) 221-240.
- [16] M. Hochburck, C. Lubich, On Krylov subspace approximations to the matrix exponential operator, *SIAM J. Numer. Anal.* 34 (1997) 1911-1925.
- [17] G. M. Homsy, Model equations for wavy viscous film flow, *Lect. in Appl. Math.* 15 (1974) 191-194.
- [18] J. M. Hyman, B. Nicolaenko, The Kuramoto-Sivashinsky equation: a bridge between PDE's and dynamical systems, *Physica D.* 18 (1986) 113-126.
- [19] P. L. Kapitza, Wave flow in thin layer of viscous liquid, *Zh. Exp. Theor. Fiz.* 18 (1948) 3-18.
- [20] A. K. Kassam, L. N. Trefethen, Fourth-order time stepping for stiff PDEs, *SIAM J. of Sci. Comput.* 26 (4) (2005) 1214-1233.
- [21] A. H. Khater, R. S. Temsah, Numerical solutions of the generalized Kuramoto-Sivashinsky equation by Chebyshev spectral collocation methods, *Comput. Math. Appl.* 56 (2008) 1465-1472.
- [22] D. J. Korteweg, G. de Vries, On the change of form of long waves advancing in a rectangular canal, and on a new type of long stationary waves, *Phil. Mag.* 39 (1895) 422-443.
- [23] S. Krogstad, Generalized integrating factor methods for stiff PDEs, *J. Comput. Phys.* 203 (2005) 72-88.
- [24] Y. Kuramoto, T. Tsuzuki, Persistent propagation of concentration waves in dissipative media far from thermal equilibrium, *Prog. Theor. Phys.* 55 (1976) 356.
- [25] H. Lai, C. F. Ma, Lattice Boltzmann method for the generalized Kuramoto-Sivashinsky equation, *Physica A.* 388 (2009) 1405-1412.
- [26] M. Lakestania, M. Dehghan, Numerical solutions of the generalized Kuramoto-Sivashinsky equation using B-spline functions, *Appl. Math. Model.* 36 (2012) 605-617.
- [27] S. K. Lele, Compact finite difference schemes with spectral-like resolution *J. Comput. Phys.* 103 (1) (1992) 16-42.
- [28] A. V. Manickam, K. M. Moudgalya, A. K. Pani, Second-order splitting combined with orthogonal cubic spline collocation method for the Kuramoto-Sivashinsky equation, *Comput. Math. Appl.* 35 (1998) 5-25.
- [29] R. C. Mittal, G. Arora, Quintic B-spline collocation method for numerical solution of the Kuramoto-Sivashinsky equation, *Commun. Nonlinear Sci. Numer. Simul.* 15 (2010) 2798-2808.
- [30] C. Moler, C. Van Loan, Nineteen dubious ways to compute the exponential of a matrix, twenty-five years later, *SIAM Rev.* 45 (2003) 3-49.
- [31] A. Mouloud, H. Fellouah, B. A. Wade, M. Kessal, Time discretization and stability regions for dissipative-dispersive Kuramoto-Sivashinsky equation arising in turbulent gas flow over laminar liquid, *J. Comput. Appl. Math.* 330 (2018) 605-617.

- [32] H. Otomo, B. M. Boghosian, F. Dubois, Efficient lattice Boltzmann models for Kuramoto-Sivashinsky equation, *Comput. Fluids*. In press.
- [33] A. Pumir, P. Manneville, Y. Pomeau, On the solitary waves running down an inclined plane, *J. Fluid Mech.* 135 (1983) 27-50.
- [34] T. Shlang, G. I. Sivashinsky, Irregular flow of a liquid film down a vertical column, *J. Phys. Paris* 43 (1982) 459-466.
- [35] G. I. Sivashinsky, Nonlinear analysis of hydrodynamics instability in laminar flames – I. derivation of basic equations, *Acta Astronaut.* 4 (1977) 1177-1206.
- [36] G. I. Sivashinsky, Instabilities, pattern-formation, and turbulence in flames, *Ann. Rev. Fluid Mech.* 15 (1983) 179-199.
- [37] G. I. Sivashinsky, D. M. Michelson, On irregular wavy flow of a liquid film down a vertical plane, *Prog. Theor. Phys.* 63 (1980) 2112-2114.
- [38] Y. A. Suhov, A spectral method for the time evolution in parabolic problems, *J. Sci. Comput.* 29 (2006) 201-217.
- [39] H. Tal-Ezer, On restart and error estimation for Krylov approximation of $w = f(A)v$, *SIAM J. Sci. Comput.* 29 (2007) 2426-2441.
- [40] M. Uddin, S. Haq, Siraj-ul-Islam, A mesh-free numerical method for solution of the family of Kuramoto-Sivashinsky equations, *Appl. Math. Comput.* 212(2) (2009) 458-469.
- [41] Y. Xu, C. W. Shu, Local discontinuous Galerkin methods for the Kuramoto-Sivashinsky equations and the Ito-type coupled KdV equations, *Comput. Meth. Appl. Mech. Eng.* 195 (2006) 3430-3447.
- [42] M. Zarebnia, R. Parvaz, Septic B-spline collocation method for numerical solution of the Kuramoto-Sivashinsky equation, *Int. J. Math. Comput. Sci. Eng.* 2 (1) (2013) 55-61.